Application of Nodal Discontinuous Glaerkin Methods in Acoustic Wave Modeling

Xin Wang

ABSTRACT

This work will explore the discontinuous Galerkin finite element method (DG-FEM) for solving acoustic wave equations in heterogeneous material. High order convergence of DG-FEM will be verified by examples. The numerical error using DG-FEM has the same components as using finite-difference method: grid dispersion and misalignment between numerical grids and material interfaces. Both error components can be reduced by high order schemes and mesh techniques respectively as I expect. The numerical experiments suggest two possible techniques to eliminate the error component associated with the mesh misalignment. The absorbing boundary conditions are implemented for infinite or semi-infinite domain problems. Plane wave as well as point source wave experiments are constructed to make validity and convergence tests of DG.

INTRODUCTION

In physics, the acoustic wave equation, governing the acoustic wave propagation through material media, describes the evolution of acoustic pressure and particle velocity as a function of space and time. Seismologists gain the knowledge of geological structure of subsurface by sending seismic waves and recording the reflected wave. Inversion of these recorded data is essential for geoscientists to understand the mystery under the surface of earth. In each inversion process, many forward wave propagation problems need to be solved. So accurately and efficiently solving acoustic wave equation is the first step for constructing an inverse solver.

FDTD for simulation of acoustic wave propagation have been studied by (Alford et al., 1974(2); Alterman and Karal, 1968(3); Boore, 1970(5), 1972(6); Dablain, 1986(8); Kelly et al., 1976(11)). There are many successful implementations of FDTD within seismic applications. Among them, the very recent software iwave by (Igor Terentyev, 2008(15)), providing a parallel framework using staggered-grid finite difference method, sets up an instrument for comparing FDTD with other numerical methods.

DG-FEM has recently become popular for fluid dynamics and electromagnetic problems

and draw more and more attention, because it provides a framework for constructing high-order scheme on general grids. DG-FEM were first proposed and analyzed in the early 1970's for solving partial differential equation (PDE). A DG-FEM method was introduced to solve the hyperbolic neutron transport equation by (Reed and Hill, 1973(13)). The first numerical analysis for a linear advection equation was presented by (Lesaint and Raviart, 1974(12)). The convergence analysis shows that the optimal convergence rate is $\mathcal{O}(h^{N+1/2})$ on general grids (Johnson and Pitkaranta, 1986(10)), where h is cell size and N is the order of local polynomial approximation. In addition, DG-FEM satisfies the physical laws behind the equation, especially convection-dominated PDEs in a close sense to finite volume method (FV) through numerical flux which gives people more flexibility to ensure the numerical stability. For linear system, such as acoustic wave equation and Maxwell's equations, the simple upwind-type numerical flux exhibits good performance.

There are two distinct types of DG-FEM: nodal (Hesthaven and Warburton, 2002(9)) and modal. In this thesis, only nodal DG-FEM is considered. In nodal DG-FEM, by carefully choosing basis functions and interpolation points, the mass matrix actually become diagonal, which costs nothing to convert. This property has certain advantage over traditional finite element method, and is good for parallel computing.

Usually, FDTD works on uniform grids. (Symes and Vdovina, 2008(14); Brown 1984(7)) pointed out that higher order scheme can control the higher order error of grid dispersion, but a first-order error component due to mesh misalignment would not be eliminated by higher order scheme. For layered material with straight line interface, conventional (regular-grid) FDTD may resolve this error component by forcing grid points to put along the interfaces. This technique doesn't work for staggered-grid finite difference method any more, because several computational grids are employed. In practice, the material medium often has complex structure and curved interface. DG-FEM suffers this predicament when the grid misaligns with the material interface. There are techniques on mesh level to suppress this first-order component. One is to use mesh generation softwares that can put the mesh grids along the interface. Another one is to refine the mesh near the interface so that grid size h is relatively smaller. The first technique has some restrictions because it depends on the mesh generation software you use and the material structure. In contrast, local refinement technique can automatically refine the grid points near the interface according to the material information from any initial mesh.

Infinite or semi-infinite domain problems arise either because the physical domain is infinite or semi-infinite, or the physical domain is relatively large in comparison with the domain of interest. Reflections of outgoing wave can cause wrong solution. Absorbing boundary

conditions are the artificial boundary condition to minimize the artificial reflection from the boundary of the domain and therefore ensure the stability of numerical schemes. A perfectly matched layer (PML), originally formulated by (Berenger, 1994(4)) for Maxwell's equations, is designed to absorb outgoing incident wave from any incidence angle. Since then, several reformulations of PML have been constructed and applied in FDTD, finite element method and DG-FEM. In this thesis, a formulation of PML proposed by (Abarbanel and Gottlieb, 1998(1)) is implemented.

In the following section, the original acoustic wave equations and PML version will be introduced. I will illustrate a simple DG-FEM construction for a modal problem as well as an upwind-type numerical flux for acoustic wave equations. The numerical experiments include plane wave and point source wave examples.

GOVERNING EQUATIONS

We consider the governing equations describing acoustic wave propagation in 2-D,

$$\begin{aligned} \rho(x,y)\frac{\partial u}{\partial t}+\frac{\partial p}{\partial x} &= 0 \\ \rho(x,y)\frac{\partial v}{\partial t}+\frac{\partial p}{\partial y} &= 0 \\ \frac{1}{\kappa(x,y)}\frac{\partial p}{\partial t}+\frac{\partial u}{\partial x}+\frac{\partial v}{\partial y} &= S(x,y,t) \end{aligned} \tag{1}$$

subject to initial conditions and boundary conditions, where p is acoustic pressure; (u,v) is particle velocity; S is a source term; ρ and κ are density and bulk modulus, respectively; $c=\sqrt{\kappa/\rho}$ is sound speed; t is time variable; $(x,y)\in\Omega$ are spatial variables.

A PML version of acoustic wave equations proposed by (Abarbanel and Gottlieb, 1998(1)) is stated as

$$\begin{aligned} \frac{\partial u}{\partial t}+2\eta_x u+\frac{1}{\rho}\frac{\partial p}{\partial x} &= \eta_x P_x \\ \frac{\partial v}{\partial t}+2\eta_y v+\frac{1}{\rho}\frac{\partial p}{\partial y} &= \eta_y P_y \\ \frac{\partial p}{\partial t}+\kappa\nabla\cdot\mathbf{v} &= \kappa S-\eta_{x_p}Q_x-\eta_{y_p}Q_y \\ \frac{\partial P_x}{\partial t}+\eta_x u=0 \qquad & \qquad \frac{\partial P_y}{\partial t}+\eta_y v=0 \\ \frac{\partial Q_x}{\partial t}+\eta_x Q_x=\kappa u \qquad & \qquad \frac{\partial Q_y}{\partial t}+\eta_y Q_y=\kappa v. \end{aligned} \tag{2}$$

(P_x, P_y, Q_x, Q_y) are four auxiliary variables.

$$\eta_\alpha = \begin{cases} \eta_{\alpha_{max}} \Big(\dfrac{\frac{L_\alpha}{2} + \alpha}{d} \Big)^2 & \alpha \in [-d - \dfrac{L_\alpha}{2}, -\dfrac{L_\alpha}{2}] \\ 0 & \alpha \in (-\dfrac{L_\alpha}{2}, \dfrac{L_\alpha}{2}] \\ \eta_{\alpha_{max}} \Big(\dfrac{\frac{L_\alpha}{2} - \alpha}{d} \Big)^2 & \alpha \in (\dfrac{L_\alpha}{2}, \dfrac{L_\alpha}{2} + d] \end{cases},$$

$$\eta_{\alpha_p} = \frac{d\eta_\alpha}{d\alpha}$$

where $\alpha \in \{x, y\}$, and $\{L_x, L_y\}$ is the domain size, and d is the PML thickness.

DG-FEM CONSTRUCTION

For simplicity, I consider 1-D scalar conservation law

$$\frac{\partial u}{\partial t} + \frac{\partial f(u)}{\partial x} = 0$$

After multiplying a test function v, integrating over the interval D^k and applying the integration by part, I have

$$\int_{D^k} \frac{\partial u}{\partial t} v dx + [f^* v]_{x^{k-1}}^{x^k} = \int_{D^k} \frac{\partial v}{\partial x} f(u) dx, \forall v \in L_2(D^k),\ D^k := [x^{k-1}, x^k] \tag{3}$$

where f^* is called numerical flux, whose definition varies according to the dynamics of the original problem .

The local solution approximation and flux approximation on D^k with polynomial basis functions are,

$$u_h^k(x,t) = \sum_{i=1}^{N} u_h^k(x_i^k, t) l_i^k(x) = \sum_{i=1}^{N} u_i^k(t) l_i^k(x), \quad l_i^k \in \mathcal{P}_{N-1}(D^k), \tag{4}$$

and

$$f_h^k(u_h^k(x,t)) = \sum_{i=1}^{N} f(u_i^k(t)) l_i^k(x), \quad l_i^k \in \mathcal{P}_{N-1}(D^k), \tag{5}$$

respectively, where $\mathcal{P}_N(D^k)$ is Nth order polynomial space on D^k. $l_i^k(x), i = 1, \cdots, N$ are Lagrange polynomials defined on N points within D^k.

Substituting u with u_h in Eq.(3) and applying integration by part once again, I get DG scheme for 1-D scalar conservation law in strong form,

$$\int_{D^k} \frac{\partial u_h^k}{\partial t} l_i^k + \frac{\partial f_h^k}{\partial x} l_i^k \; DC = [(f_h^k - f^*) l_i^k]_{x^{k-1}}^{x^k} \tag{6}$$

NUMERICAL FLUX

Let's first rewrite Eq.(1) into the matrix-vector form,

$$\mathcal{Q}\frac{\partial \mathbf{q}}{\partial t} + \mathcal{A}_x \frac{\partial \mathbf{q}}{\partial x} + \mathcal{A}_y \frac{\partial \mathbf{q}}{\partial y} = \mathbf{f}, \tag{7}$$

where

$$\mathcal{Q} = \begin{bmatrix} \rho & 0 & 0 \\ 0 & \rho & 0 \\ 0 & 0 & 1/\kappa \end{bmatrix}, \; \mathcal{A}_x = \begin{bmatrix} 0 & 0 & 1 \\ 0 & 0 & 0 \\ 1 & 0 & 0 \end{bmatrix}, \; \mathcal{A}_y = \begin{bmatrix} 0 & 0 & 0 \\ 0 & 0 & 1 \\ 0 & 1 & 0 \end{bmatrix}, \; \mathbf{q} = \begin{bmatrix} u \\ v \\ p \end{bmatrix}, \mathbf{f} = \begin{bmatrix} 0 \\ 0 \\ S \end{bmatrix} \tag{8}$$

Define $\mathcal{A}_\mathbf{n} := \mathbf{n} \cdot (\mathcal{A}_x, \mathcal{A}_y)$, where $\mathbf{n} = (n_x, n_y)$ is a unit vector. It can be easy to verify that the eigenvalues of $\mathcal{Q}^{-1}\mathcal{A}_\mathbf{n}$ is given as,

$$\lambda_1 = -c, \; \lambda_2 = 0, \; \lambda_3 = c.$$

The wave corresponding to λ_1 is entering the domain, the wave corresponding to λ_3 is leaving, and λ_2 corresponds to a stationary wave as illustrated in Fig. (1).

If introducing $c_\pm$ as the values of $c(x)$ on two sides of the interface, I can recover the *Riemann jump conditions*, also known as the *Rankine-Hugoniot conditions*, as

$$\begin{aligned} c_- \mathcal{Q}_-(\mathbf{q}^* - \mathbf{q}_-) + (\Pi\mathbf{q})^* - (\Pi\mathbf{q})_- &= 0 \\ (\Pi\mathbf{q})^* - (\Pi\mathbf{q})^{**} &= 0 \\ -c_+ \mathcal{Q}_+(\mathbf{q}^{**} - \mathbf{q}_+) + (\Pi\mathbf{q})^{**} - (\Pi\mathbf{q})_+ &= 0. \end{aligned} \tag{9}$$

where, $\mathbf{q}^*$ and $\mathbf{q}^{**}$ refers to the intermediate state, $(\Pi\mathbf{q})^*$ is the numerical flux along $\mathbf{n}$, and

$$\Pi\mathbf{q} := \mathcal{A}_n\mathbf{q} = \begin{pmatrix} n_x p \\ n_y p \\ n_x u + n_y v \end{pmatrix}. \tag{10}$$

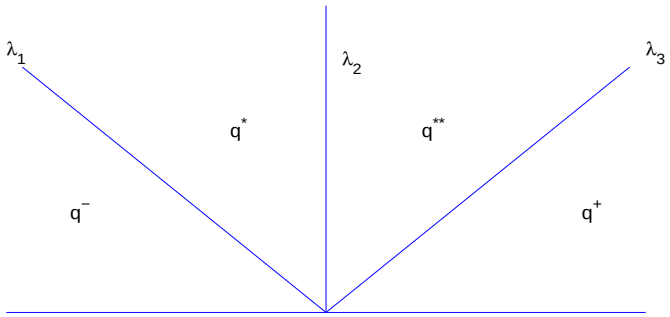

Figure 1: Sketch of the characteristic wave speeds of a three-wave system at a boundary between two state, q^- and q^+. The two intermediate system, q^* and q^{**}, are used to derive the upwind flux. In this case, $\lambda_1 < 0, \lambda_2 = 0, \lambda_3 > 0$.

By coupling the solution of Eq.(9) with the central flux, I therefore recover the numerical flux for Eq.(1)

$$\begin{aligned} \mathbf{n}_- \cdot (\mathbf{u}_- - \mathbf{u}^*) &= \frac{1}{2\{\{Z\}\}}[Z_+ \mathbf{n}_- \cdot (\mathbf{u}_- - \mathbf{u}_+) - \alpha(p_- - p_+)] \\ n_{x-}(p_- - p^*) &= -\frac{Z_-}{2\{\{Z\}\}} n_{x-}[\alpha Z_+ \mathbf{n}_- \cdot (\mathbf{u}_- - \mathbf{u}_+) - (p_- - p_+)] \\ n_{y-}(p_- - p^*) &= -\frac{Z_-}{2\{\{Z\}\}} n_{y-}[\alpha Z_+ \mathbf{n}_- \cdot (\mathbf{u}_- - \mathbf{u}_+) - (p_- - p_+)] \end{aligned} \tag{11}$$

where $Z = \sqrt{\frac{\rho\kappa}{\rho_0\kappa_0}} = \frac{\rho c}{\rho_0 c_0}$ is the relative *acoustic impedance* and $\{\{Z\}\} = \frac{Z_- + Z_+}{2}$. The parameter α in the numerical flux can be used to control dissipation; for example, taking $\alpha = 0$ yields a non-dissipative central flux and $\alpha = 1$ results in the classic upwind flux. One is free, however, to take α to be any value in between.

NUMERICAL EXPERIMENTS

Plane Wave

I consider a problem with discontinuous coefficients. Assume that the coefficients are constant except at one point $x = x_0$, where there is a jump. I denote by (ρ_L, c_L) and (ρ_R, c_R) the density and the speed of sound at the two sides of the discontinuity. The solution can be

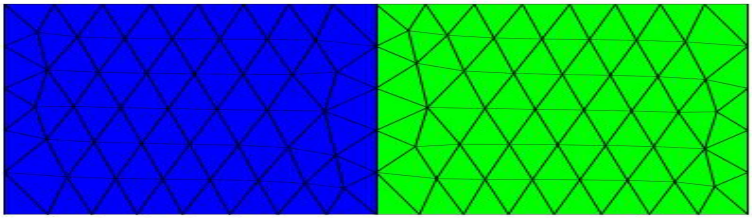

Figure 2: blue and green stand for two material. The mesh grid is shown on the background. Here, I align the grid points with the interface.

analytically expressed as,

$$\begin{aligned}
x < x_0 \quad &: \\
p(x,y,t) &= f(t - \frac{x-x_0}{c_L}) - \frac{\rho_L c_L - \rho_R c_R}{\rho_L c_L + \rho_R c_R} f(t + \frac{x-x_0}{c_L}) \\
u(x,y,t) &= \frac{1}{\rho_L c_L}(f(t - \frac{x-x_0}{c_L}) + \frac{\rho_L c_L - \rho_R c_R}{\rho_L c_L + \rho_R c_R} f(t + \frac{x-x_0}{c_L})), \\
x_0 \le x \quad &: \\
p(x,y,t) &= \frac{2\rho_R c_R}{\rho_L c_L + \rho_R c_R} f(t - \frac{x-x_0}{c_R}), \\
u(x,y,t) &= \frac{2}{\rho_L c_L + \rho_R c_R} f(t - \frac{x-x_0}{c_R}),
\end{aligned} \tag{12}$$

where f is a continuous function.

In the first experiment, I used the computation domain $[-3,-3]\times[-1,1]$ and $f = \sin(2\pi x)$. The other parameters are

$$\begin{aligned}
&x_0 = 0, \\
&\rho_L = 1.0, \quad \rho_R = 0.5, \\
&c_L = 1.0, \quad c_R = 2, \\
&time = 2, \quad no\ source\ term.
\end{aligned}$$

Next, the computation domain is set as $[0, 1800\ m] \times [-15\ m, 15\ m]$ and I choose

$$\begin{aligned}
&\rho_L = 2100\ kg/m^3, \quad c_L = 2.3\ m/ms \\
&\rho_R = 2300\ kg/m^3, \quad c_R = 3.0\ m/ms \\
&time = 600ms, \qquad no\ source\ term
\end{aligned}$$

and f is a Ricker's wavelet with central frequency $f_0 = 10\ Hz$:

$$f(t) = (1 - 2(\pi f_0(t - t_0))^2)e^{-(\pi f_0(t-t_0))^2}.$$

Table 1: convergence test for sine wave with mesh aligned with interface

h	N	$\|p_h - p\|_\infty$	$\|u_h - u\|_\infty$	$\|v_h - v\|_\infty$	R
0.2	1	0.2865	0.3232	0.1123	1.84
0.1	1	0.0799	0.1009	0.0303	1.98
0.05	1	0.0203	0.0265	0.0078	-
0.2	2	0.0402	0.0628	0.0204	2.61
0.1	2	0.0066	0.0094	0.0030	2.91
0.05	2	8.76e-4	0.0012	3.95e-4	-

Here N indicates the polynomial order in DG method, and $R = \dfrac{\log \|p_H - p\| - \log \|p_h - p\|}{\log H - \log h}$

I use three set of mesh grids to test this example: mesh aligned with interface as shown in Fig.(2), mesh misaligned with interface, local refined mesh near the interface as shown in Fig.(3).

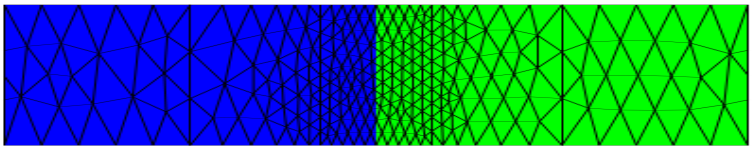

Figure 3: mesh grid with local refinement near the interface.

Table 2: convergence test for Ricker's wavelet with mesh aligned with interface

h	N	$\|p_h - p\|_\infty$	$\|u_h - u\|_\infty$	$\|v_h - v\|_\infty$	R
10	1	0.0125	0.0154	0.0045	2.51
5	1	0.0022	0.0037	0.0012	1.86
2.5	1	6.04e-4	1.00e-3	3.14e-4	-
10	2	9.81e-4	0.0014	3.17e-4	2.96
5	2	1.26e-4	1.85e-4	4.14e-5	2.96
2.5	2	1.62e-5	2.34e-5	5.23e-6	-

I also investigate the behavior of a train of plane waves impinging on the interface and entering the absorbing layer, i.e. PML, as described by Eq.(2). In this experiment, I used the domain $[-3, 3] \times [-1, 1]$ and the PML layer $[2, 3] \times [-1, 1]$. Then $L_x = 4$. The other parameters are

$$\begin{aligned} &\rho_L = 1.0, \quad && \rho_R = 0.5, \\ &c_L = 1.0, \quad && c_R = 2, \\ &time = 2, \\ &f = sin(x), \quad && no\ source\ term. \end{aligned}$$

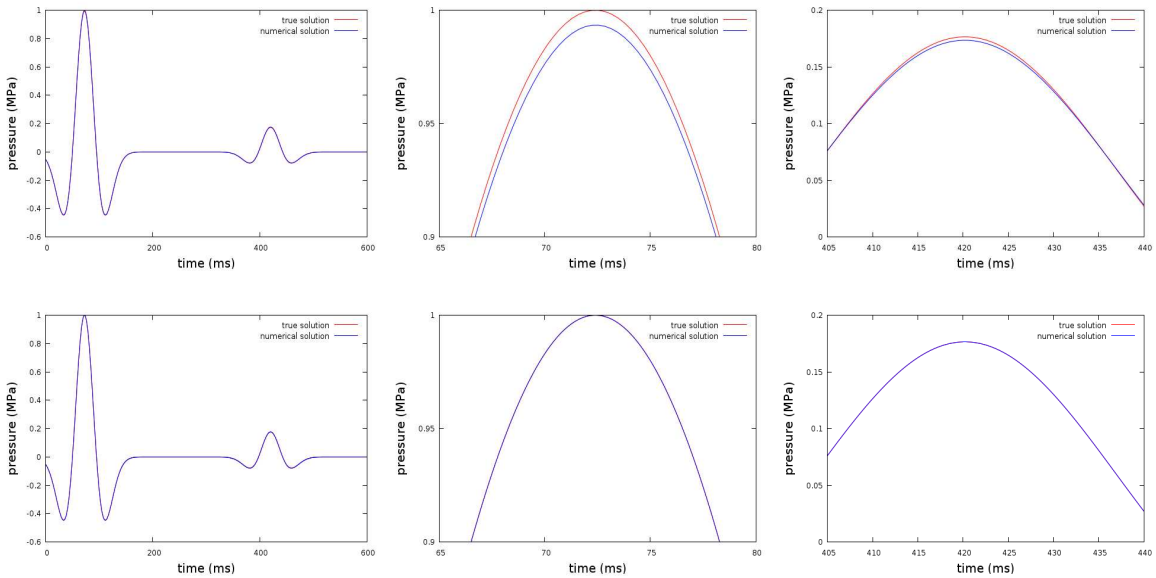

Figure 4: traces of the true and numerical solutions at 500 m, $h = 10$ m, the grid points align with the interface as shown in Fig.(2) polynomial order $N = 1$ in the top three figures, $N = 2$ in the bottom three figures.

One can find the analytic solution for this example based on the paper by (Abarbanel and Gottlieb, 1998(1)).

Table 3: convergence test for sine wave with PML

h	N	$\|p_h - p\|_\infty$	$\|u_h - u\|_\infty$	$\|v_h - v\|_\infty$	R
0.2	1	0.2278	0.2966	0.1015	1.58
0.1	1	0.0764	0.0983	0.0298	1.51
0.05	1	0.0268	0.0322	0.0078	-
0.2	2	0.0519	0.0692	0.0224	2.89
0.1	2	0.0070	0.0096	0.0031	2.98
0.05	2	8.89e-4	0.0012	4.07e-4	2.99
0.025	2	1.12e-4	1.57e-4	5.11e-5	-

Point Source Wave

Here, I investigate the performance of DG-FEM for point source wave propagation problem. I use zero initial conditions in both experiments. The boundary conditions are free

surface boundary conditions and PML, respectively. The computation domain is $[-0.5, 0.5] \times [-0.5, 0.5]$; $\rho = 1.0$, $\kappa = 1.0$; The point source is located at $x_s = (0, 1/4)$ with expression,

$$S(x,t) = (t - t_0)e^{-(\pi f_0(t-t_0))^2}\delta(x - x_s)$$

where $f_0 = 10$, $t_0 = 1.2/f_0$. The receiver is located at $(0, -1/4)$. In the experiment with PML, the PML layers with thickness 0.2 are wrapped around the computation domain.

DISCUSSION

Through numerical examples, DG-FEM appears to achieve the optimal convergence rate. In the plane wave example, higher-order scheme controls the error that leads to grid dispersion. The misalignment between mesh grid and material interface causes a first-order error component, which can not be eliminated by high order schemes. This is consistent with mathematical analysis in FDTD by (Symes and Vdovina, 2008(14)). I propose two mesh techniques to overcome this problem. One is to align the mesh grid along the interface. Another is to use local mesh refinement near the interface. Numerical experiments show that both techniques give me better results. In addition, DG-FEM works well for point source wave propagation, even though I actually use polynomials to approximate Dirac delta function. In future, I will finish the mesh refinement code which can automatically refine the mesh around the interface according to the material information provided by geoscientists. I will also construct 3-D examples.

REFERENCES

[1] S. Abarbanel and D. Gottlieb. On the construction and analysis of absorbing layers in CEM. *Appl. Numer. Math.*, 27:331–340, 1998.

[2] R. M. Alford, K. R. Kelly, and D. M. Boore. Accuracy of finite-difference modeling of the acoustic wave equation. *Geophysics*, 39:834–842, 1974.

[3] Z. Alterman and F. C. Karal. Propagation of elastic waves in layered media by finite difference methods. *Bull. Seismol. Soc. Am.*, 58:367–398, 1968.

[4] J. P. Berenger. A perfectly matched layer for the absorption of electromagnetic waves. *Journal of Computational Physics*, 114:185–200, 1994.

[5] D. M. Boore. Love waves in non-uniform wave guides: finite difference calculations. *Geophys. Res.*, 75:1512–1527, 1970.

[6] D. M. Boore. Finite dierence methods for seismic wave propagation in heterogeneous materials. *Chapter 1 in Methods in Computational Physics, II.*, 1972.

[7] David L. Brown. A note on the numerical solution of the wave equation with piecewise smooth coefficients. *Mathematics of Computation*, 42(166):369–391, 1984.

[8] M. A. Dablain. The application of high-order dierencing to the scalar wave equation. *Geophysics*, 51:54–66, 1986.

[9] J. S. Hesthaven and T. Warburton. Nodal high-order methods on unstructured grids i. time-domain solution of maxwell's equations. *Journal of Computational Physics*, 181(1):186–221, 2002.

[10] C. Johnson and J. Pitkaranta. An analysis of the discontinuous galerkin method for a scalar hyperbolic equation. *Math. Comp.*, 46:1–26, 1986.

[11] K. R. Kelly, R. W. Ward, S. Treitel, and R. M. Alford. Synthetic seismograms: a nite-dierence approach. *Geophysics*, 41:2–27, 1976.

[12] P. Lesaint and P. A. Raviart. On a finite element method for solving the neutron transport equation. *In mathematical aspects of finite elements in partial differential equations*, Academic Press, New York:89–145, 1974.

[13] W. H. Reed and T. R. Hill. Triangular mesh methods for the neutron transport equation. *Los Alamos Scientific Laboratory Report*, LA-UR-73-479, 1973.

[14] William W. Symes and Tetyana Vdovina. Interface error analysis for numerical wave propagation. *TR08-22*, 2008.

[15] Igor Terentyev. iwave, The Rice Inversion Project, Rice University, 2008.

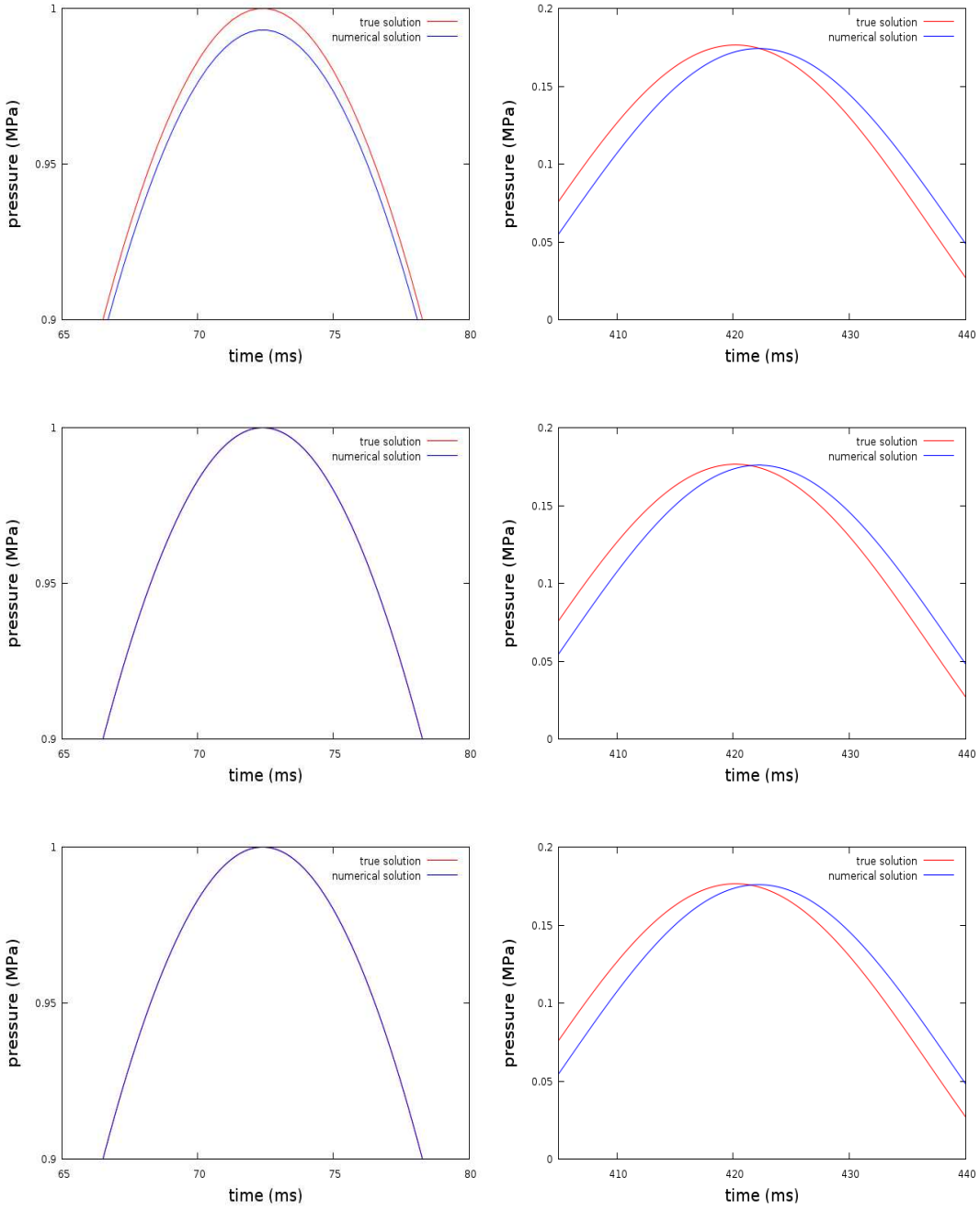

Figure 5: traces of the true and numerical solutions at 500 m, $h = 10$ m, the grid points don't align with the interface, $N = 1$ in the top two figures, $N = 2$ in the middle two figures, $N = 4$ in the bottom two figures. the higher order schemes can not eliminate the error component due to the mesh misalignment.

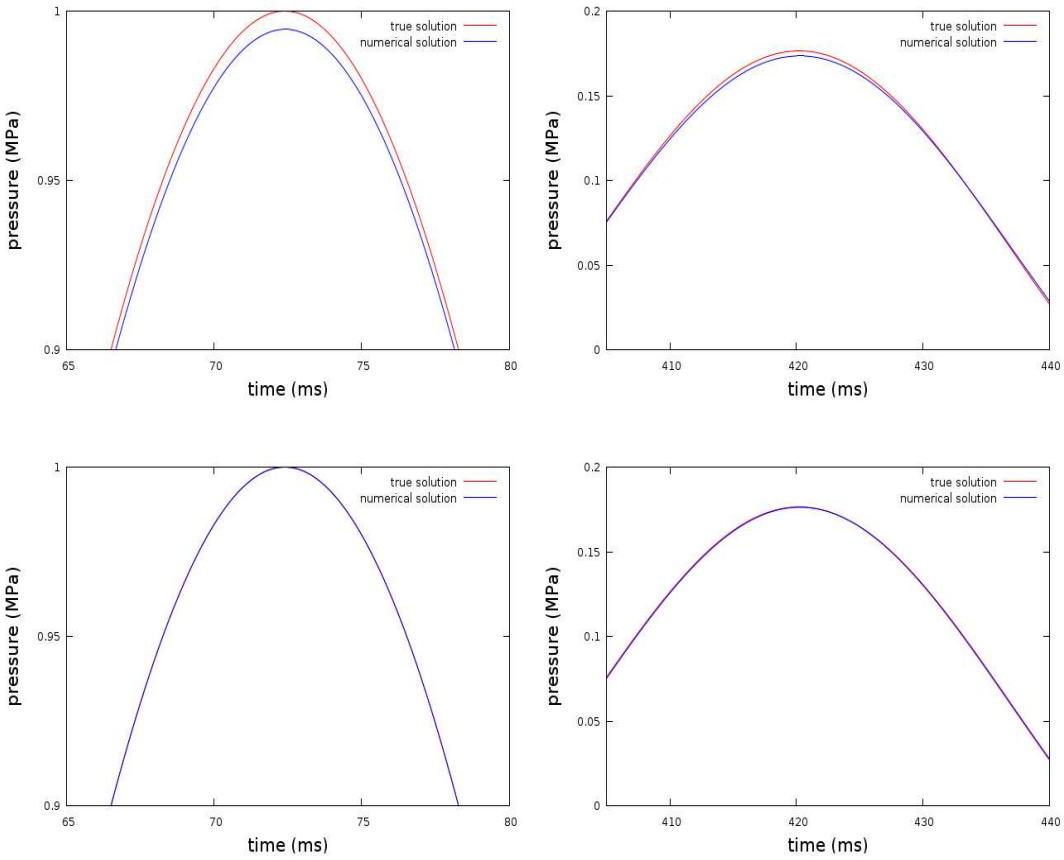

Figure 6: traces of the true and numerical solutions at 500 m, $h = 10$ m, the grid points is locally refined near the interface as shown in Fig.(3) $N = 1$ in the top two figures, $N = 2$ in the bottom two figures.

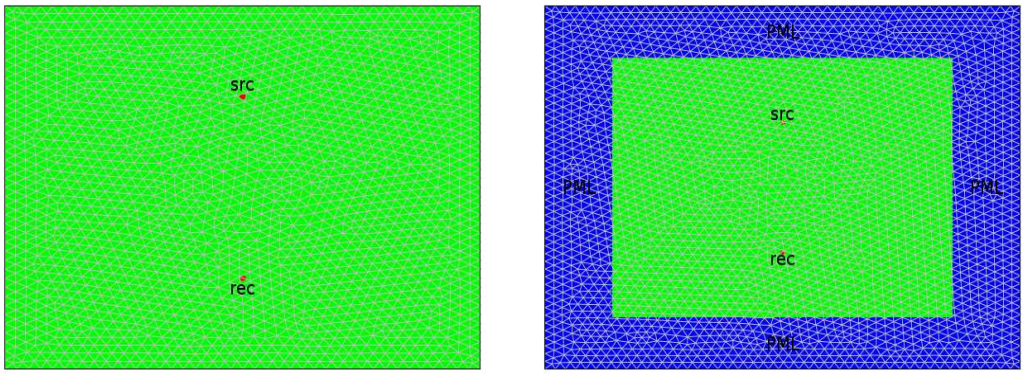

Figure 7: the computation domain for point source wave propagation. the left one is for the free surface boundary example; the right one is for the PML example.

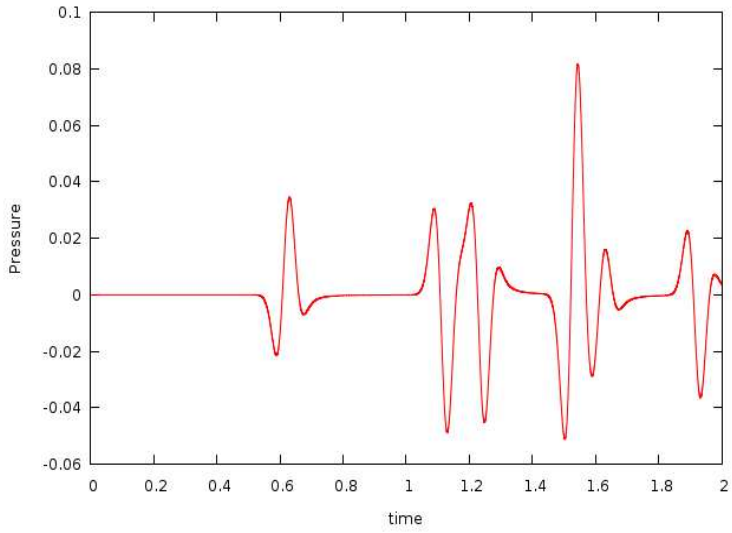

Figure 8: The trace of analytic solution at $(0, -0.25)$ for free surface boundary conditions, generated by FORTRAN code acfree.f by Thomas Hagstrom.

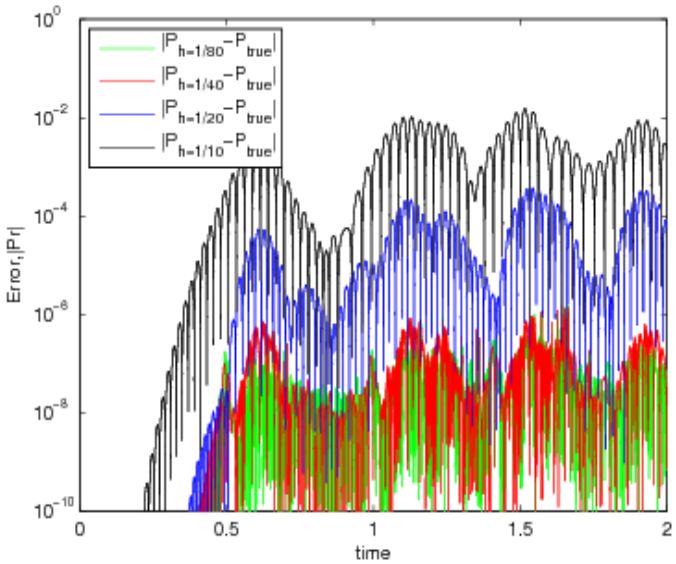

Figure 9: trace error of analytic solution and numerical solution with free surface boundary conditions, $N = 5$, $h = 1/10, 1/20, 1/40, 1/80$.

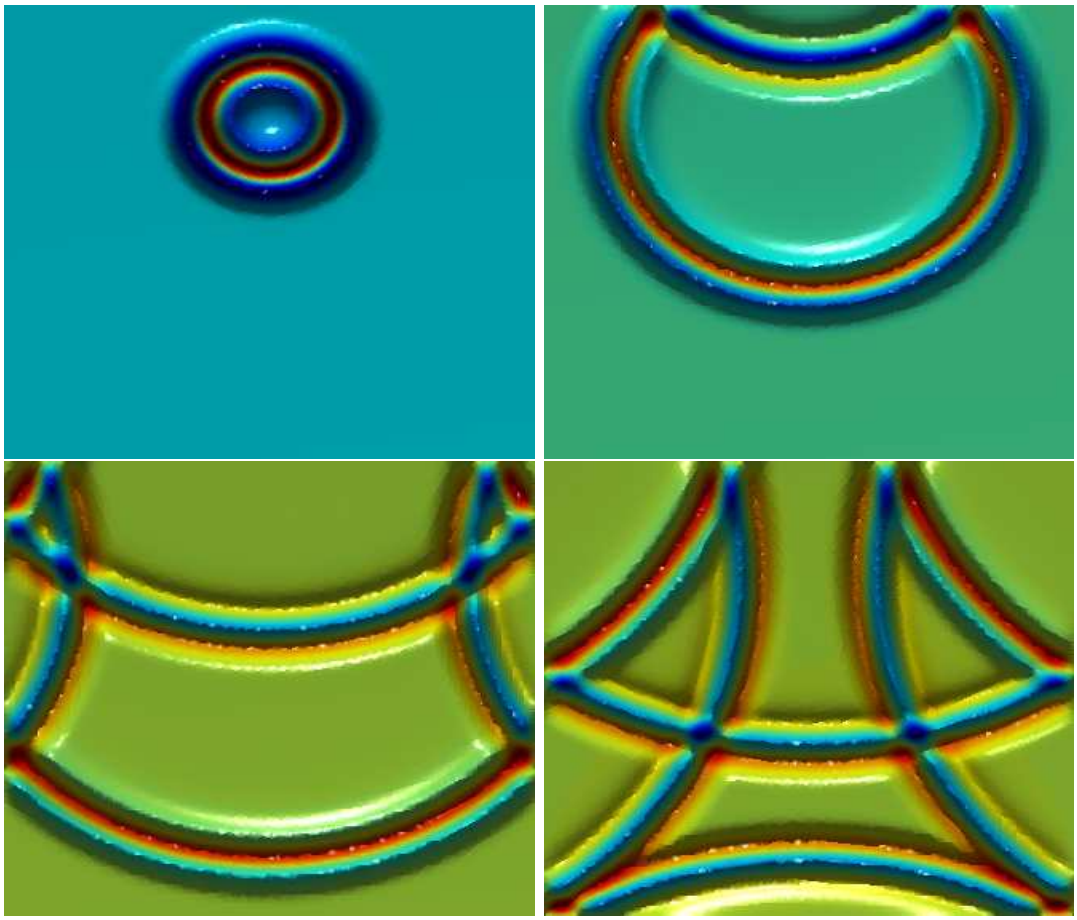

Figure 10: the pressure contour of source wave propagation at different time with free boundary conditions. the upper-left figure, $t = 0.25$; the upper-right figure, $t = 0.50$; the lower-left figure, $t = 0.75$; the lower-right figure $t = 1.0$. $N = 3$, $h = 0.25$.

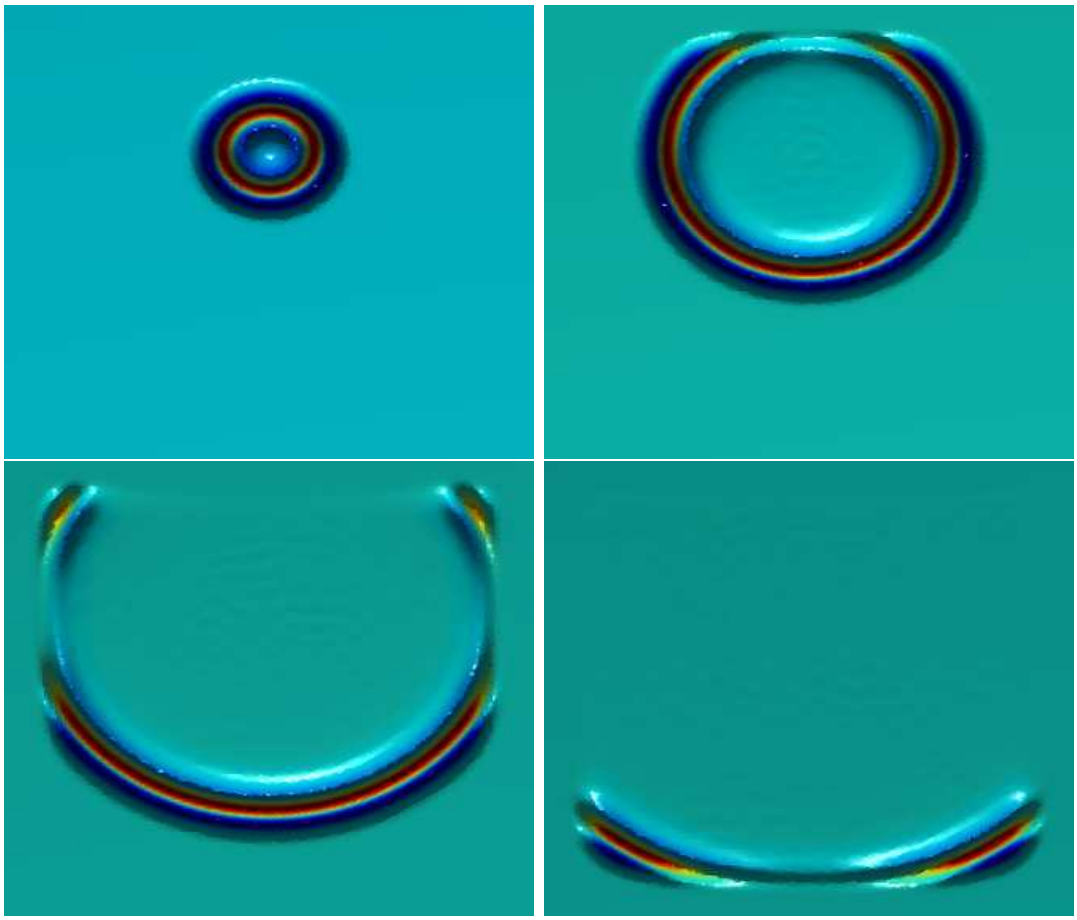

Figure 11: the pressure contour of source wave propagation at different time with PML. the upper-left figure, $t = 0.25$; the upper-right figure, $t = 0.50$; the lower-left figure, $t = 0.75$; the lower-right figure $t = 1.0.N = 3$,$h = 0.30$.